Electronic structure and localized lanthanide character of LnT_2Al_{10} (T = Ru, Os)

H. Tanida,[1] D. Tanaka,[1] M. Sera,[1] S. Tanimoto,[2] T. Nishioka,[2] M. Matsumura,[2] M. Ogawa,[3] C. Moriyoshi,[3] Y. Kuroiwa,[3] J. E. Kim,[4] N. Tsuji,[4] and M. Takata[5]

[1]*Department of ADSM, Hiroshima University, Higashi-Hiroshima 739-8530, Japan*

[2]*Department of Physics, Kochi University, Kochi, Japan*

[3]*Department of Physical Science, Hiroshima University, Higashi-Hiroshima 739-8526, Japan*

[4]*JASRI/SPring-8, Sayou, Hyogo 676-5198, Japan*

[5]*RIKEN/SPring-8, Sayou, Hyogo 679-5148, Japan*

(Received 29 June 2011; published 21 September 2011)

The high-energy synchrotron x-ray powder diffraction experiments of $LaRu_2Al_{10}$ were carried out to clarify the charge-density distribution, which is derived by the maximum entropy method/Rietveld technique. The results indicate that the charge density between Ru and surrounding Al atoms is large, but that between La and surrounding Al atoms is small. We propose that the Ru-Al_{10} polyhedron is the fundamental component of the crystal and the two-dimensional layer is constructed by these polyhedra in the *ac* plane and is stacked along the *b* axis by way of the Al5 atom. The Ln ion is located inside the crevice formed by the surrounding Ru-Al_{10} polyhedra and behaves as a nearly free ion. We studied the thermal and magnetic properties of NdT_2Al_{10} (T = Ru, Os), which exhibits the antiferromagnetic order at T_N = 2.4 and 2.2 K for T = Ru and Os, respectively. We observed a small lattice distortion below T_N, which indicates the small coupling between the orbital moment of the Nd ion and the lattice. The results of the magnetic susceptibility indicate the small crystalline electric field effect. These results mean that the Nd ion behaves as a nearly free ion, which is supported by the results of the charge-density distribution of $LaRu_2Al_{10}$.

DOI: 10.1103/PhysRevB.84.115128 PACS number(s): 75.30.Mb, 75.20.Hr, 71.27.+a

I. INTRODUCTION

Ce-based compounds have been studied extensively due to the interesting phenomena originating from the strong electron-electron correlation. The Kondo semiconductor is one of the systems with such an interesting physics. Recently, CeT_2Al_{10} (T = Ru, Os, Fe), which is categorized into the Kondo semiconductor, have attracted much attention because of the unusual long-range order in $CeRu_2Al_{10}$ and $CeOs_2Al_{10}$. LnT_2Al_{10} crystallizes into the orthorhombic $YbFe_2Al_{10}$-type structure.[1,2] Among this series of compounds, CeT_2Al_{10} (T = Ru, Os, Fe) have been studied extensively.[3–27] Strydom reported the macroscopic properties of $CeRu_2Al_{10}$ and proposed the antiferromagnetic (AFM) order at 27 K.[3] Muro *et al.* reported the physical properties of $CeFe_2Al_{10}$, which do not show the magnetic order down to low temperature.[4] From the results of the electrical resistivity, CeT_2Al_{10} is categorized into a Kondo semiconductor. The detailed studies on this system using the single crystals were performed by Nishioka *et al.*[5] Although the shortest distance between Ce ions is as large as 5.2 Å, the transition temperature T_0 is extremely high, 27.3 and 28.7 K in $CeRu_2Al_{10}$ and $CeOs_2Al_{10}$, respectively. These are much higher than T_N = 16 K in $GdRu_2Al_{10}$.[5] Considering that the magnetic order of $GdRu_2Al_{10}$ is understood by the usual exchange interaction, the origin of the transition in CeT_2Al_{10} is expected to be different from that in $GdRu_2Al_{10}$. Tanida *et al.* proposed the long-range order with a singlet ground state,[7] which was consistent with the inelastic neutron scattering results that a spin gap with a large excitation energy of 8 meV was observed in the ordered state in $CeRu_2Al_{10}$.[14] The spin gap was also observed in $CeOs_2Al_{10}$.[16] However, soon after, the neutron scattering experiments of $CeRu_2Al_{10}$ revealed that the AFM order with a small antiferromagnetic moment (m_{AF}) of 0.42μ_B/Ce parallel to the *c* axis takes place below T_0.[15,20,25] This AFM order is quite mysterious because T_0 is too high for the small ordered moment and $m_{AF} \parallel c$ below T_N is not simply expected from $\chi_a > \chi_c > \chi_b$ in the paramagnetic region.[5,10,13] Here, χ_a means the magnetic susceptibility χ along the *a* axis, etc. Very large pressure effect on CeT_2Al_{10} was revealed by Nishioka *et al.*[5] By applying pressure to $CeRu_2Al_{10}$, the physical properties easily change from the nearly localized nature in $CeRu_2Al_{10}$ to a valence fluctuation regime in $CeFe_2Al_{10}$. $CeOs_2Al_{10}$ is located just between the above two compounds. This indicates that, although a distance between Ce ions is large, the *c*-*f* hybridization effect should play an important role in the unusual long-range order. It should be noted that the unusual increase of T_0 of $CeRu_2Al_{10}$ by applying pressure, which is different from the suppression of the transition temperature by pressure observed in a usual Kondo compound. As for the electronic structure of $CeRu_2Al_{10}$, we proposed two-dimensional nature in the *ac* plane, which is stacked along the *b* axis through Al5 atoms from the comparison between the lattice constants between $CeRu_2Al_{10}$ and $CeFe_2Al_{10}$ and the anisotropic transport properties.[10] Very recently, Kimura *et al.* reported the optical conductivity of $CeOs_2Al_{10}$ and proposed that the charge-density wave transition along the *b* axis appears at ∼40 K and the magnetic order at T_0 = 29 K is driven by the electronic instability.[22] Quite recently, Kondo *et al.* reported the high-field magnetization of $CeOs_2Al_{10}$ and proposed that the spin gap accompanied with a singlet ground state begins to appear at ∼40 K, where the charge gap appears at the same time and the singlet component coexists with the AFM moment in the ordered state and the strong coupling between spin and charge degrees of freedom of electron is essential in the mysterious transition in CeT_2Al_{10}.[24]

Although the extensive studies on the CeT_2Al_{10} system have been performed, as for the physical properties of other LnT_2Al_{10} compounds, little has been known; we note that

the magnetic susceptibilities of $LnFe_2Al_{10}$ polycrystals have been studied systematically.[1] It is important to investigate the electronic state of this series of compounds. Especially, the information on the anisotropy of the charge-density distribution of the constituent atoms is important to clarify how the bonding is between atoms in the crystal structure and how the circumstances are of the Ln atom. Recently developed maximum entropy method (MEM)/Rietveld technique, which is a combination of MEM and Rietveld refinement, could successfully derive the charge-density distribution of many compounds from which the information on the electronic structure could be derived.[28–30] Although, in a metallic compound, the information on the conduction electron could not be derived by the MEM/Rietveld analysis, the information on the anisotropic bonding by means of the inner core electrons could be derived. In this paper, we performed the high-energy synchrotron x-ray powder diffraction of $LaRu_2Al_{10}$ and derived the charge-density distribution by the MEM/Rietveld technique.

It is also important to investigate the physical properties of NdT_2Al_{10}, which is considered as a well-localized compound as a reference magnetic compound for CeT_2Al_{10}, and by comparing the results with those of CeT_2Al_{10} with much higher transition temperatures, the information on the origin of the unusual long-range order in CeT_2Al_{10} could be derived. In order to obtain the information on the Nd ion in NdT_2Al_{10} (T = Ru, Os), we studied their magnetic and thermal properties.

II. EXPERIMENT

The single crystals of NdT_2Al_{10} (T = Ru, Os) were prepared by an Al flux method. To accurately determine the crystal structure, particularly at the electron charge-density levels, it is essential to collect accurate Bragg intensity data. For this purpose, a high-energy synchrotron powder diffraction experiment at $T = 300$ K was carried out at BL02B2 in SPring-8 using the large Debye-Sherrer camera equipped with an imaging plate as a two-dimensional detector. High-energy x rays with wavelength $\lambda = 0.66823(4)$ Å were used as incident x rays. After grinding $LaRu_2Al_{10}$ powder in an agate mortar, the homogeneous granularity of the sample powder, which gave a homogeneous intensity distribution in the Debye-Sherrer powder ring, was achieved by the precipitation method. The $LaRu_2Al_{10}$ powder was sealed in a borosilicate capillary of 0.1 mm internal diameter for diffraction measurement. The electron-density distribution was determined by the MEM/Rietveld method. The magnetic susceptibility of NdT_2Al_{10} was measured by SQUID magnetometer Quantum Design Magnetic Property Measurement System (MPMS). The magnetization of NdT_2Al_{10} at low temperatures was measured by the extraction method up to $H = 10$ T. The thermal expansion of $NdOs_2Al_{10}$ was measured by a three-terminal capacitance method at low temperatures.

III. EXPERIMENTAL RESULTS

A. Structure refinements and charge-density distribution of $LaRu_2Al_{10}$

The powder diffraction pattern of $LaRu_2Al_{10}$ was analyzed by the Rietveld method for the data in $2\theta < 74.5°$ ($d > 0.55$ Å). The results of the profile fitting for the data of

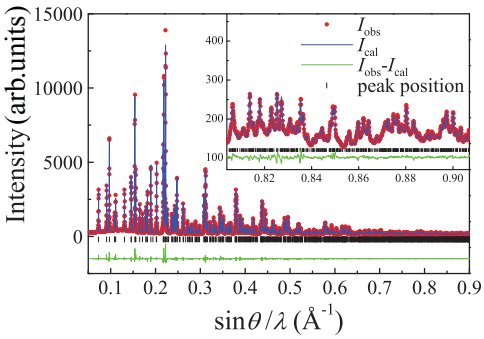

FIG. 1. (Color online) Result of the Rietveld refinement of $LaRu_2Al_{10}$. The reliability factors $R_{wp} = 3.874\%$, $R_I = 1.864\%$, and $R_F = 1.163\%$. The deviation between the observed intensity and calculation is drawn at the bottom of figure with the indications of peak position. A closeup in the high-angle region is depicted in the inset.

$LaRu_2Al_{10}$ at $T = 300$ K are shown in Fig. 1. The space group is $Cmcm$. The fitting was successfully done even at the high-angle region as shown in the inset of Fig. 1. The obtained reliability factors based on the weighted profile R_{wp}, integrated intensity R_I, and structure factor R_F were 3.874%, 1.864%, and 1.163%, respectively. The crystal-structure parameters refined by the Rietveld analysis are listed in Table I. The 1471 independent observed structure factors extracted by the Rietveld analysis were used in the MEM analysis.

The selected interatomic distances in the structure of $LaRu_2Al_{10}$ are listed in Table II. The distance between La and other atoms is large, which is typically ~3.2 Å. On the other hand, those between Ru and other atoms are small, which is typically ~2.6 Å. Those between Al atoms are typically ~2.8 Å.

The MEM analysis of $LaRu_2Al_{10}$ was carried out with the unit cell divided into $92 \times 92 \times 92$ pixels. The volume of one pixel corresponds to approximately $0.1 \times 0.1 \times 0.1$ Å^3. The three-dimensional (3D) charge-density distribution of $LaRu_2Al_{10}$ at 300 K is shown in Fig. 2. The equi-electron-density surface level is $0.3e$ Å^{-3}, although the information on the conduction electron could not be obtained. However, the information on the anisotropic charge density between constituent atoms could be obtained from the present results. It is easily found that the charge density between Ru and Al5

TABLE I. Atomic coordinates (x, y, z) and isotropic displacement parameter U of $LaRu_2Al_{10}$ at 300 K refined by the Rietveld analysis. Space group is $Cmcm$ (No. 63). The orthorhombic lattice parameters are $a = 9.15452(3)$ Å, $b = 10.29964(4)$ Å, and $c = 9.21471(3)$ Å.

Atom	Site	x	y	z	$U \times 10^2$ (Å^2)
La	4c	0	0.12304(5)	0.25	0.67(1)
Ru	8d	0.25	0.25	0	0.66(1)
Al1	8g	0.2259(2)	0.3640(2)	0.25	0.86(4)
Al2	8g	0.3514(2)	0.1298(2)	0.25	0.95(4)
Al3	8f	0	0.1628(2)	0.6015(2)	0.92(5)
Al4	8f	0	0.3791(2)	0.0520(2)	1.24(4)
Al5	8e	0.2286(2)	0	0	1.03(4)

TABLE II. Selected interatomic distances in the structure of $LaRu_2Al_{10}$. Symmetry code: (i) $x+1/2, y+1/2, z$; (ii) $-x, -y, -z$; (iii) $x, y, -z+1/2$; (iv) $-x+1/2, y+1/2, -z+1/2$; (v) $-x+1/2, -y+1/2, -z$; (vi) $-x, y, -z+1/2$; (vii) $-x, -y, -z$.

Bond	Length (Å)	Bond	Length (Å)
La-Al1	3.231(2)	Al1-Al2	2.672(3)
La-Al1^{i}	3.662(2)	Al1-Al2^{iv}	2.827(3)
La-Al2	3.217(2)	Al1-Al3^{v}	2.872(2)
La-Al3	3.264(2)	Al1-Al4	2.762(2)
La-Al3^{ii}	3.247(2)	Al1-Al5^{v}	2.7280(10)
La-Al4	3.207(2)	Al2-Al3^{v}	2.880(2)
La-Al5	3.3604(10)	Al2-Al4^{v}	3.099(2)
		Al2-Al5	2.8906(2)
La-Ru	3.5007(2)	Al3-Al4^{iii}	2.639(3)
		Al3-Al5^{vi}	2.840(2)
Ru-Al1	2.5952(8)	Al4-Al5^{v}	2.820(2)
Ru-Al2	2.7752(10)	Al2-Al2^{vi}	2.722(2)
Ru-Al3^{iii}	2.6304(8)	Al3-Al3^{iii}	2.738(2)
Ru-Al4	2.6899(11)	Al4-Al4^{vii}	2.668(3)
Ru-Al5	2.58235(12)		

atoms is large and the La atom is isolated from the surrounding Al and Ru atoms.

More detailed information is obtained from Figs. 3(a)–3(c), which show the charge-density distribution projected on the *bc*, *ab*, and *ac* planes, respectively. It is found that all the atoms exhibit the anisotropic charge-density distribution, from which the information on the anisotropic bonding between the constituent atoms could be derived. In the *bc* plane, the equicontour charge-density maps of the (400) and (100) planes are shown. In the (400) plane on which Ru, Al1, and Al5 atoms are located, it is clearly seen that the charge density between Ru-Al5 atoms along the *b* axis and that between Ru-Al1 atoms along the *c* axis is large. It is also seen that the charge density of Ru atom expands toward the Al2 atom. In the (100) plane on which La, Al3, and Al4 atoms are located, the charge density between La and the surrounding atoms is small. Thus, the La atom is found to be isolated in the (100) plane. As for the anisotropic charge-density distribution of Al atoms, the

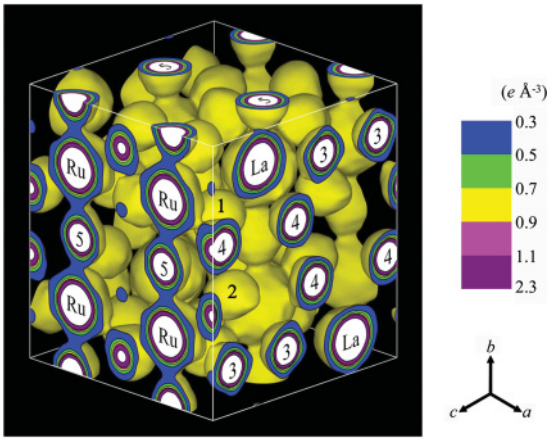

FIG. 2. (Color online) Electron charge-density distribution of $LaRu_2Al_{10}$ at $T = 300$ K. The equi-electron-density surface level in the three-dimensional map is $0.3e$ Å^{-3}.

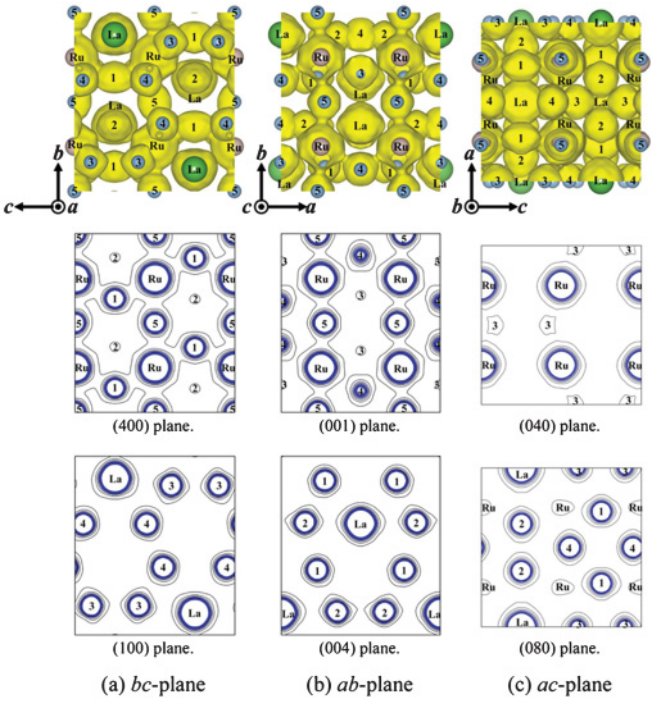

FIG. 3. (Color online) Charge density of $LaRu_2Al_{10}$ in the (a) *bc* plane, (b) *ab* plane, and (c) *ac* plane at $T = 300$ K. The upper figures are the charge density projected on *bc*, *ab*, and *ac* planes, where the equidensity surface at $0.3e$ Å^{-3} is shown. Constituent atoms are shown as a ball. The name of five Al atoms from Al1 to Al5 is abbreviated from 1 to 5, respectively. The middle and lower ones are those in specific planes indicated in the figures, where the contour lines are drawn from $0.3e$ Å^{-3} with $0.1e$ Å^{-3} intervals.

following characteristics are observed. In the (400) plane, that of the Al1 atom is symmetric against the *b* axis and that of the Al5 atom is asymmetric against both *b* and *c* axes. In the (100) plane, Al3 and Al4 atoms are asymmetric against both *b* and *c* axes. The Al3 atom takes a squarelike charge-density distribution, the vertex axes of which are deviated from the *b* or *c* axis. The vertex along the *c* axis expands toward the La atom and the nearest Al3 atom. The charge density also expands toward the Al4 atom. Thus, a squarelike charge-density distribution is rotated in the *bc* plane. This may originate from the fact that the *y* coordinate of two Al3 atoms is deviated from that of the La atom along the *c* axis such that the *y* coordinate of the Al3 atom is 0.1628 and that of the La atom is 0.12304. This difference makes the charge-density distribution of Al3 atoms rotate in the *bc* plane so as to get the hybridization energy gain between La, Al3, and Al4 atoms. Although the charge-density distribution of the Al4 atom is rather isotropic, it is seen that it expands toward the La, Al3, and nearest Al4 atoms. While both the Al3 and Al4 atoms look isolated in the *bc* plane, there exists $\rho_{\min}$ of $\sim 0.3e$ Å between the Ru-Al3 atoms and between the Ru-Al4 atoms as is seen in Fig. 4. In the *ab* plane, the equicontour charge-density maps of (001) and (004) planes are shown. The charge density between Ru-Al5 atoms along the *b* axis is large as in the *bc* plane. The charge density of the Ru atom expands toward the Al5, Al4, and also Al3 sites. As for the anisotropic charge-density distribution of Al atoms, the following characteristics are observed. Those of

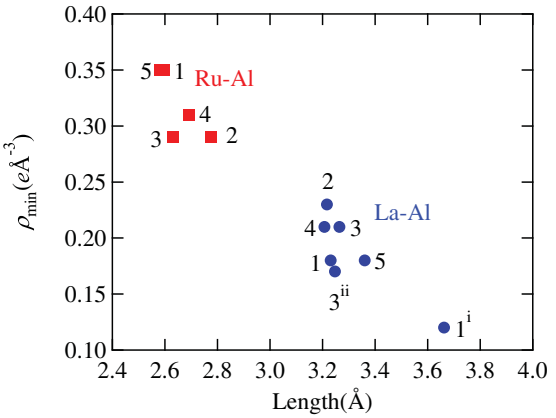

FIG. 4. (Color online) Length dependence of the minimum charge density between two different ions ρ_{min} of $LaRu_2Al_{10}$. Red squares and blue circles indicate ρ_{min} between Ru and Al and that between La and Al, respectively.

the Al4 and Al5 sites are symmetric against the *b* and *a* axes in the (001) plane, respectively. In the (004) plane, those of the Al1 and Al2 sites are asymmetric against both *a* and *b* axes. While the Al4 atom looks isolated in the (100) plane, its charge density expands toward the Ru atom in the (001) plane, which leads to the large charge density between Ru-Al4 atoms along the *a* axis. While the La atom looks isolated as is seen in the (100) plane, it is seen in the (004) plane that its charge density expands toward both sides of the Al2 atoms along the *a* axis. The Al2 atom exhibits a modified squarelike charge-density distribution, which expands toward the La and Al2 atoms along the *a* axis and toward the Al1 atom. The ρ_{min} between the Al2-La atoms is largest among those between La and Al atoms and also ρ_{min} between the Al2 atoms is largest among those between the nearest Al sites. The ρ_{min} between the Al2 atoms is $0.28e$ Å^{-3}, which is comparable with those between the Ru-Al3 or Ru-Al2 atoms. The charge density of the Al1 atom is rather isotropic in the (004) plane. However, it is seen that its charge density expands toward the La and neighboring Al2 atoms. The charge density of the Al2 atom is slightly asymmetric against the *b* axis, although it is much less pronounced than that of the Al3 atom in the *bc* plane. The asymmetric charge-density distribution of Al2 originates from the deviation of the *x* and *y* coordinates from that of the La atom. The *y* coordinates of the La and Al2 atoms are 0.12304 and 0.1298, respectively, which are smaller than the difference of the *y* coordinates of the La and Al3 atoms in the *bc* plane.

In the *ac* plane, the equicontour charge-density maps of (040) and (080) planes are shown. In the (040) plane, the Al1 atom exhibits a largely anisotropic charge density, which expands toward the Ru atom along the *c* axis, although the *y* coordinate is deviated largely between the Ru and Al1 atoms. It is also seen that the charge density of the Ru atom expands toward the Al3 atom, although it is small due to the large deviation of the *z* coordinate between the Al3 and Ru atoms. In the (080) plane, it is seen that the charge density of the La atom expands toward the Al2 atom along the *a* axis and, also, the large charge density exists between the nearest Al2 atoms as is seen in the (004) plane.. As for the anisotropic charge-density distributions, those of the Al1 and Al2 atoms are symmetric against the *a* axis. Those of the Al3 and Al4 atoms are symmetric against the *c* axis. The former is because the *z* coordinate (=0.25) of Al1 and Al2 atoms is the same as that of the La atom. The latter is because the *x* coordinate (=0) of the Al3 and Al4 atoms is the same as that of the La atom.

The minimum charge densities ρ_{min} between the Ru and nearest Al atoms and those between the La and nearest Al atoms are shown in Fig. 4 as a function of their interatomic distances. Generally, the shorter the interatomic distance, the larger ρ_{min}. The ρ_{min} between Ru-Al atoms is large and that between the La and Al atoms is small. Among ρ_{min} between Ru-Al atoms, the largest ρ_{min} exists between Ru-Al1 atoms and also between Ru-Al5 atoms. The ρ_{min} between Ru-Al4 atoms are intermediate. The ρ_{min} between Ru-Al2 atoms and that between Ru-Al3 atoms are smallest. The former comes from its largest bond length among the Ru-Al bondings. Also in the La-Al bondings, there exists the same general tendency that the shorter the interatomic distance, the larger ρ_{min}. The largest ρ_{min} of $0.23e$ Å^{-3} exists between La-Al2 atoms and the smallest one of $0.18e$ Å^{-3} between La-Al5 atoms and between La-Al1 atoms. Here, we note the interesting tendency that the larger the charge density between Ru-Al atoms, the smaller the charge density between La-Al atoms. The ρ_{min} between Ru-Al5 atoms is largest among those between Ru-five Al atoms, and that between La-Al5 atoms is smallest among those between La-five Al atoms. This means that the Al5 atom is most largely affected by the Ru atom and the effect from the La atom is smallest. The ρ_{min} between Ru-Al2 atoms is smallest among those between Ru-five Al atoms and that between La-Al2 atoms is largest among those between La-five Al atoms. This means that the Al2 atom is most largely affected by the La atom and the effect from the Ru atom is smallest. The average of ρ_{min} between Ru-five Al atoms and that between La-five Al atoms is nearly the same, which is between $0.25\sim0.27e$ Å^{-3}.

B. Magnetic and thermal properties of NdT_2Al_{10} (T = Ru, Os)

Figures 5(a) and 5(b) show the temperature (T) dependence of χ and χ^{-1} of $NdRu_2Al_{10}$ and $NdOs_2Al_{10}$ measured at $H = 1$ T along the three crystal axes, respectively. Both compounds show very similar behavior. χ exhibits the relation of $\chi_a > \chi_c > \chi_b$ in a wide range of temperature, which is the same as that in CeT_2Al_{10}.[5,10,13] Above ~100 K, a Curie-Weiss behavior is observed. The effective Bohr magneton μ_{eff} obtained from the result above ~100 K is ~3.65 μ_B/Nd, which is close to the value expected from a free Nd ion. This suggests that the overall CEF splitting is small. A pronounced hump is observed at ~20 K along the *b* axis, which suggests that the first excited CEF level is located at ~60 K above the CEF ground state. Here, we note the characteristic T dependence of χ_c. In $NdRu_2Al_{10}$, although the relation of $\chi_a > \chi_c > \chi_b$ remains up to 300 K, χ_c becomes close to χ_b above ~200 K. In $NdOs_2Al_{10}$, the same tendency is seen and, at ~230 K, χ_b becomes larger than χ_c.

Figures 6(a) and 6(b) show the T dependence of the magnetization (M) along the *a* axis M_a of $NdRu_2Al_{10}$ and $NdOs_2Al_{10}$ at low temperatures, respectively. M_a measured at $H = 1$ T shows a peak at 2.3 and 2.2 K in $NdRu_2Al_{10}$ and $NdOs_2Al_{10}$, respectively. The transition temperature decreases

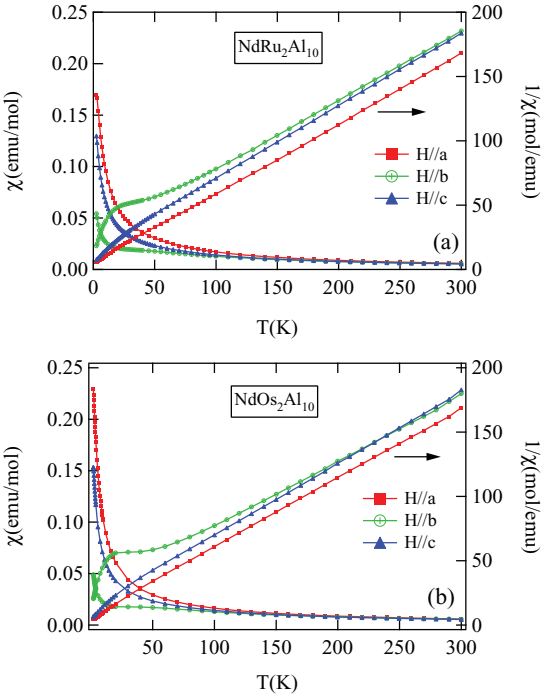

FIG. 5. (Color online) Temperature dependence of the magnetic susceptibility and inverse magnetic susceptibility of (a) $NdRu_2Al_{10}$ and (b) $NdOs_2Al_{10}$ along the three crystal axes.

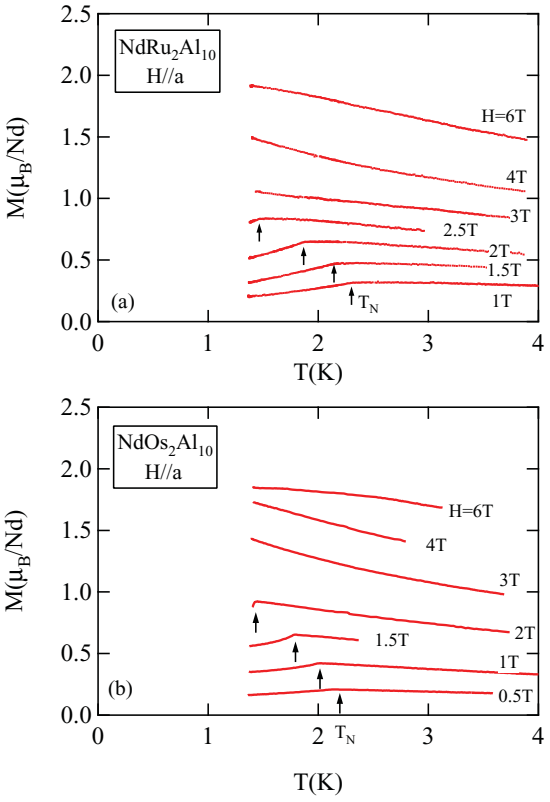

FIG. 6. (Color online) Temperature dependence of magnetization of $NdOs_2Al_{10}$ along the a axis.

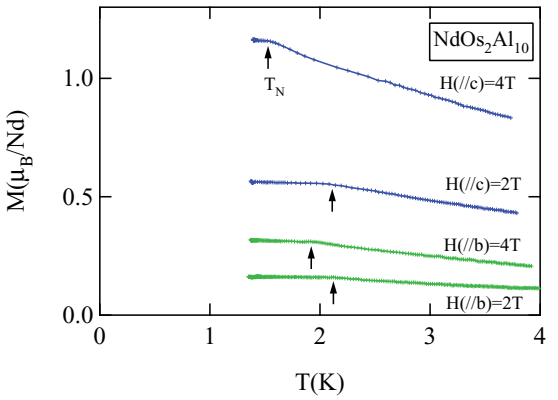

FIG. 7. (Color online) Temperature dependence of the magnetization of $NdOs_2Al_{10}$ along the b and c axes at $H = 2$ and 4 T.

with increasing magnetic field. Above $H = 3$ T, M_a shows a monotonous increase with decreasing temperature. At $H = 6$ T, a saturated behavior is seen with decreasing temperature. As will be shown later, the T dependence of M for $H \parallel b$ and c below the transition temperature is almost independent of temperature. These results suggest that the AFM order with the component of $m_{AF} \parallel a$ takes place below $T_N = 2.4$ and 2.2 K in $NdRu_2Al_{10}$ and $NdOs_2Al_{10}$, respectively.

Figure 7 shows the T dependence of M_b and M_c of $NdOs_2Al_{10}$ at $H = 2$ and 4 T. The T dependence of M_b and M_c below T_N is very weak. $NdRu_2Al_{10}$ shows similar results. These results of M_a, M_b, and M_c indicate that the AFM order with the component of $m_{AF} \parallel a$ is realized below T_N in NdT_2Al_{10}.

Figure 8 shows the magnetization curves of $NdOs_2Al_{10}$ along the three crystal axes at $T = 1.4$ K. $NdRu_2Al_{10}$ exhibits similar behavior. M_a shows a concave H dependence up to $H_c = 2.1$ and 2.6 T in $NdOs_2Al_{10}$ and $NdRu_2Al_{10}$, respectively. This concave H dependence of M originates from the existence of the $\chi_\parallel$ component. Above H_c, M shows a roughly H-linear increase up to ~4 T and a saturated behavior above ~5 T after showing a shoulder at ~4.5 T. We note that a shoulder at ~5 T does not originate from the phase transition, but the H region above H_c is paramagnetic. On the other hand, M_b and M_c show an H-linear increase up to H_c and a saturated behavior above H_c. There, the magnitude of the slope of M/H is much smaller for $H \parallel b$ than for $H \parallel c$. The

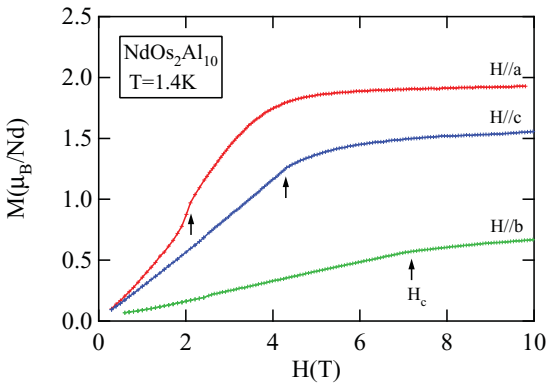

FIG. 8. (Color online) Magnetization curves of $NdOs_2Al_{10}$ at $T = 1.4$ K along the three crystal axes.

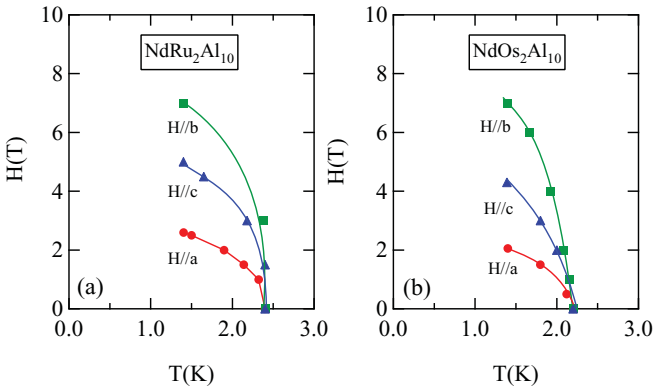

FIG. 9. (Color online) Magnetic phase diagram of (a) $NdRu_2Al_{10}$ and (b) $NdOs_2Al_{10}$.

similar magnetization curves along the three crystal axes are observed also in $NdRu_2Al_{10}$.

Figures 9(a) and 9(b) show the magnetic phase diagrams of $NdRu_2Al_{10}$ and $NdOs_2Al_{10}$, respectively. Both compounds show the similar magnetic phase diagram. Below T_N, the AFM ordered state with the anisotropic H_c is realized. H_c along the b axis is largest and H_c along the a axis is smallest.

Figure 10 shows the thermal expansion of $NdOs_2Al_{10}$ along the three crystal axes in zero magnetic field. The a and c axes expand, and the b axis shrinks below $T_N = 2.2$ K. The magnitude of the lattice distortion below T_N is as small as 10^{-6}. This indicates that the coupling between the orbital moment of the Nd ion and the lattice is very small.

IV. DISCUSSION

First, we discuss the electronic structure of $LaRu_2Al_{10}$ based on the results by MEM/Rietveld analysis. The results show that the charge density between Ru-Al atoms is large and that between La-Al atoms is small, as is seen in Figs. 2–4. The small charge density between La-Al atoms, which is close to the background level of the MEM charge density, indicates that the La ion is isolated and behaves as a nearly free ion. Thus, this compound could be viewed as a caged compound. Strydom proposed that the Ln atom of LnT_2Al_{10} is located inside the R_4-Al_{16} polyhedron.[3] Contrary to this picture, we propose the following one by considering the large charge

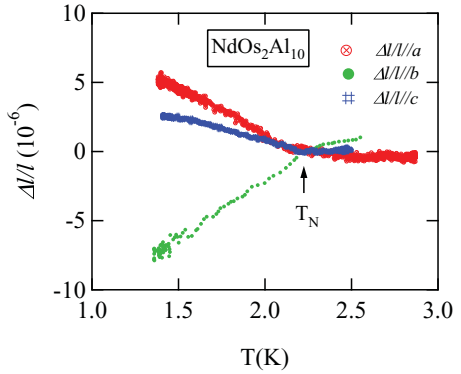

FIG. 10. (Color online) Thermal expansion of $NdOs_2Al_{10}$ along the a, b, and c axes in zero magnetic field.

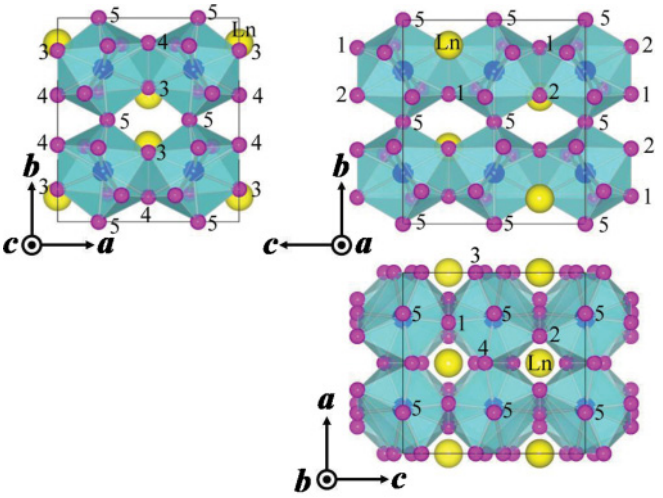

FIG. 11. (Color online) Crystal structure of LnT_2Al_{10} constructed by the Ru-Al_{10} polyhedra. Along the b axis, the Al5 atom is shared, and in the ac plane, Al1, Al2, Al3, and Al4 atoms are shared by the Ru-Al_{10} polyhedra. The big yellow circle is the La ion. The number on a small purple circle means the number of Al sites.

density between Ru-Al atoms and the small one between La-Al atoms. The Ru-Al_{10} polyhedron is the fundamental component constructing the $YbFe_2Al_{10}$-type crystal structure. Figure 11 shows the crystal structure constructed by connecting the Ru-Al_{10} polyhedra. One Al atom (Al5) is shared by the two Ru-Al_{10} polyhedra along the b axis. On the other hand, in the ac plane, the two Ru-Al_{10} polyhedra share two Al atoms (Al1, Al2) along the a axis and two Al atoms (Al3, Al4) along the c axis. Then, the total charge density between the Ru-Al_{10} polyhedra in the ac plane is larger than those along the b axis. Thus, LnT_2Al_{10} could be viewed as a two-dimensional system in the ac plane. The Ru-Al_{10} polyhedra form the two-dimensional layer in the ac plane and this layer is connected by the Al5 atom along the b axis as we proposed in our previous paper.[10] The La atom is located in the crevice formed as a result of the connection of the Ru-Al_{10} polyhedra. In the same way, the Nd ion in NdT_2Al_{10} is also expected to behave as a nearly free ion inside the crevice constructed by the surrounding Ru-Al_{10} polyhedra. This is consistent with very small lattice distortion below T_N and a small CEF effect. In such a case, although the Ln atom possibly induces a rattling vibration inside the crevice, the isotropic displacement parameter U of the La atom is small as 0.0067 Å^2 at $T = 300$ K, which is much smaller than those of Ln atoms in the filled skutterdites.[33,34] The U of the La atom is comparable with those of other constituent atoms of this compound as shown in Table I. Thus, the rattling vibration of the Ln atom is small in the LnT_2Al_{10} system. As for U of the La atom, values along the a, b, and c axes are found to be 0.0063(2), 0.0059(2), and 0.0080(2), respectively. This implies the existence of an anisotropic motion of the La atom, although their magnitudes remain weak (less than 0.01). The U along the c axis is largest. The reason could be seen in the anisotropic charge-density distribution of the La atom, which is shown in Fig. 3 and also in Fig. 4. The charge density between the La-Al2 atoms is largest, as is clearly seen in Fig. 3(b), which means that the bonding between La and Al2 atoms is strong and the La atom

is rather tightly fixed along the a axis. This makes the vibration of the La atom along the a axis small. On the other hand, the charge-density distribution of the La atoms along the c axis is small, which makes the vibration along the c axis large. As for the small U along the b axis, the strong bonding between La-Al2 atoms possibly makes the vibration along the b axis difficult.

It is interesting to compare the present results of the anisotropic charge-density distribution of five Al sites with the results of nuclear quadrupole resonance (NQR) and nuclear magnetic resonance (NMR) experiments.[6,19] We note that the NQR parameters of V_{zz} and η are similar between $CeRu_2Al_{10}$ and $LaRu_2Al_{10}$,[19] which means that the electronic structure that determines the NQR parameters are nearly the same between these two compounds. Here, V_{zz} and η are the largest principal axis of the electric field gradient tensor and the asymmetry parameter, respectively. The V_{zz} of five Al sites reflect their anisotropic charge density. Our previous report and our recent detailed NMR experiments showed the following results.[19,27] The V_{zz} of the Al1 site is almost along the a axis, but 1.7° deviated from the a axis in the ab plane. The V_{zz} of the Al2 site is almost along the a axis but 3.4° deviated from the a axis in the ab plane. The V_{zz} of the Al3 site is along the direction of 32.9° from the b axis in the bc plane. The V_{zz} of the Al4 site is along the direction of 13.6° from the c axis in the bc plane. The V_{zz} of the Al5 site is almost along the b axis but 0.6° deviated from the b axis in the bc plane. At the Al1 and Al2 sites, the charge-density distribution against the b axis in the bc plane and that against the a axis in the ac plane are symmetric, but in the ab plane, they are asymmetric. This should be associated with the results of V_{zz} of the Al1 and Al2 sites obtained by the NMR experiments. At the Al3 and Al4 sites, the charge-density distribution against the b axis in the ab plane and that against the c axis in the ac plane are symmetric, but in the bc plane, they are asymmetric. This should be associated with the results of V_{zz} of the Al3 and Al4 sites obtained by the NMR experiments. At the Al5 site, the charge-density distribution against the c axis in the ab plane is symmetric, but in the bc plane, it is asymmetric. This should be associated with the results of V_{zz} of the Al5 site obtained by the NMR experiments.

Next, we discuss the coupling between the orbital moment of the Nd ion and the lattice and also the CEF effect on the Nd ion from the surrounding atoms. The order of the lattice distortion of $NdOs_2Al_{10}$ below T_N is 10^{-6}. This is found to be very small when we compare with other compounds. For example, in NdB_6 with $T_N = 8$ K, it is 10^{-4},[31] and in CeB_6 with the same order of $T_N = 2.3$ K, it is 10^{-5}.[32] The present result indicates that the coupling between the orbital moment of the Nd ion and the lattice is very small, and the Nd ion is expected to behave as a nearly free ion. Then, the CEF effect on the Nd ion from the surrounding atoms is expected to be small. In fact, χ of NdT_2Al_{10} exhibits a Curie-Weiss behavior with $\mu_{eff} \sim 3.65\mu_B$/Nd, which is close to the expected value from a free Nd ion above ~100 K. The overall CEF splitting of NdT_2Al_{10} may be ~200 K. The T dependence of χ of the $NdFe_2Al_{10}$ polycrystal also shows a Curie-Weiss behavior with a small CEF effect.[1] Thus, all of the NdT_2Al_{10} compounds exhibit a Curie-Weiss behavior with a small CEF effect independent of the T ion. Furthermore, the systematic studies of the magnetic susceptibility of $LnFe_2Al_{10}$ polycrystals reported by Thiede *et al.*[1] showed that $LnFe_2Al_{10}$ with a well-localized Ln ion exhibits a Curie-Weiss behavior in a wide range of temperature without showing a large CEF effect. From these results, we conclude that, in all of the LnT_2Al_{10} compounds with a well-localized Ln, the CEF splitting originating from the Coulomb interaction is small, independent of Ln and T ions and the Ln ion behaves as a nearly free ion. On the other hand, the CEF splitting of CeT_2Al_{10} should be very large, which comes from the large anisotropy of χ in the paramagnetic region.[5,13,24] The overall CEF splitting of CeT_2Al_{10} is expected to be as large as $500 \sim 1000$ K from the results of χ. In CeT_2Al_{10}, the c-f hybridization effect should be important to determine the CEF splitting in place of the Coulomb interaction and is expected to be the origin of the large CEF splitting.

Finally, we briefly comment on the anisotropy of the magnetization of NdT_2Al_{10} at low temperatures. The present results show that $M_a : M_b : M_c \sim 1{:}0.4{:}0.8$ in NdT_2Al_{10} at $H = 10$ T, which is in the paramagnetic region above H_c at $T = 1.4$ K. M_b is smallest and the difference between M_a and M_c is small. The present results indicate that the AFM order with the component of $m_{AF} \parallel a$ is realized. When the isotropic exchange interaction is considered, $m_{AF} \parallel a$ is consistent with the anisotropy of $\chi_a > \chi_c > \chi_b$ in the paramagnetic region. In this sense, NdT_2Al_{10} is a normal AFM compound compared with CeT_2Al_{10}. In $CeRu_2Al_{10}$, the AFM order with $m_{AF} \parallel c$ is realized regardless of the large anisotropy such as $\chi_a : \chi_c : \chi_b = 13{:}4{:}1$ at T_0. In $CeRu_2Al_{10}$, it is necessary to introduce the anisotropic exchange interaction, which should be largest along the c axis. There, the contribution of the c-f hybridization effect should be essential. Kondo *et al.* proposed that $m_{AF} \parallel c$ regardless that $\chi_a > \chi_c > \chi_b$ originates from the largest c-f hybridization along the a axis, which makes $m_{AF} \parallel c$ in place of $m_{AF} \parallel a$ expected from $\chi_a > \chi_c$ in the paramagnetic region.[24] As information on the conduction electrons could not be derived from the MEM/Rietveld analysis, it is difficult to discuss the c-f hybridization effect in CeT_2Al_{10}. However, it may be possible to extract some information on the c-f hybridization from the present results by combining them with our very recent results of NQR (Ref. 26) and NMR.[27] The data indicate that the internal field (H_{int}) at the Al2 site is much larger than at the other four Al sites and is also much larger than the dipole field calculated by assuming the AFM ordered structure with $m_{AF} = 0.42\ \mu_B$/Ce parallel to the c axis derived by the neutron scattering experiment.[15,20,25] This large H_{int} on the Al2 site could originate from the transferred hyperfine field from the surrounding atoms. The present result of a large charge density between La-Al2 atoms could be associated with the large H_{int} on the Al2 site and possibly suggests the existence of a large c-f hybridization between Ce and Al2 atoms.

V. SUMMARY

In order to clarify the electronic structure of the present system, we performed the high-energy synchrotron x-ray powder diffraction experiments of $LaRu_2Al_{10}$. The charge-density distribution of $LaRu_2Al_{10}$ derived by the MEM/Rietveld technique indicates that the charge density between Ru and

surrounding Al ions is large, but that between La and surrounding Al ions is small. From these results, we proposed that the Ru-Al_{10} polyhedron is the fundamental component to construct the crystal structure. The two-dimensional layer is constructed by connecting the Ru-Al_{10} polyhedra in the *ac* plane, and this layer is stacked along the *b* axis by way of the Al5 atom. The La ion is inside the crevice formed by the surrounding Ru-Al_{10} polyhedra and is expected to behave as a nearly free ion from the small magnitude of the charge density between La and surrounding atoms. We studied the thermal expansion and magnetic properties of NdT_2Al_{10} (T = Ru, Os). T_N of NdT_2Al_{10} is 2.4 and 2.2 K for T = Ru and Os, respectively. We observed very small lattice distortion below T_N, which indicates the small coupling between the orbital moment of the Nd ion and the lattice. The Curie-Weiss behavior with μ_{eff} ~3.65 μ_B/Nd close to the value expected from a free Nd ion was observed above ~100 K along all the crystal axes, which indicates the small CEF splitting in NdT_2Al_{10}. Together with the systematic study of the magnetic susceptibility of $LnFe_2Al_{10}$ by Thiede *et al.*, we conclude that the CEF effect is small in LnT_2Al_{10} with a well-localized Ln ion, and the Ln ion behaves as a nearly free ion. These results of the thermal and magnetic properties are strongly supported by the results of the charge-density distribution of $LaRu_2Al_{10}$. The magnetization at low temperatures indicates that the AFM order with the component of $m_{AF} \parallel a$ is realized in NdT_2Al_{10}. $m_{AF} \parallel a$ is consistent with the anisotropy of χ in the paramagnetic region, different from the case of CeT_2Al_{10} where $m_{AF} \parallel c$ is realized regardless of $\chi_a > \chi_c > \chi_b$ in the paramagnetic region.

[1] V. M. Thiede, T. Ebel, and W. Jeitsschko, J. Mater. Chem. **8**, 125 (1998).

[2] A. I. Tursina, S. N. Nesterenko, E. V. Murashova, I. V. Chernyshev, H. Noel, and Y. D. Sropegin, Acta Crystallogr., Sect. E: Struct. Rep. Online **61**, i12 (2005).

[3] A. M. Strydom, Phys. B (Amsterdam) **404**, 2981 (2009).

[4] Y. Muro, K. Motoya, Y. Saiga, and T. Takabatake, J. Phys. Soc. Jpn. **78**, 083707 (2009).

[5] T. Nishioka, Y. Kawamura, T. Takesaka, R. Kobayashi, H. Kato, M. Matsumura, K. Kodama, K. Matsubayashi, and Y. Uwatoko, J. Phys. Soc. Jpn. **78**, 123705 (2009).

[6] M. Matsumura, Y. Kawamura, S. Edamoto, T. Takesaka, H. Kato, T. Nishioka, Y. Tokunaga, S. Kambe, and H. Yasuoka, J. Phys. Soc. Jpn. **78**, 123713 (2009).

[7] H. Tanida, D. Tanaka, M. Sera, C. Moriyoshi, Y. Kuroiwa, T. Takesaka, T. Nishioka, H. Kato, and M. Matsumura, J. Phys. Soc. Jpn. **79**, 043708 (2010).

[8] K. Hanzawa, J. Phys. Soc. Jpn. **79**, 043710 (2010).

[9] S. Kambe, H. Chudo, Y. Tokunaga, T. Koyama, H. Sasaki, T. U. Ito, K. Ninomiya, W. Higemoto, T. Takesaka, T. Nishioka, and Y. Miyake, J. Phys. Soc. Jpn. **79**, 053708 (2010).

[10] H. Tanida, D. Tanaka, M. Sera, C. Moriyoshi, Y. Kuroiwa, T. Takesaka, T. Nishioka, H. Kato, and M. Matsumura, J. Phys. Soc. Jpn. **79**, 063709 (2010).

[11] A. Kondo, J. Wang, K. Kindo, T. Takesaka, Y. Kawwamura, T. Nishioka, D. Tanaka, H. Tanida, and M. Sera, J. Phys. Soc. Jpn. **79**, 073709 (2010).

[12] H. Tanida, D. Tanaka, M. Sera, C. Moriyoshi, Y. Kuroiwa, T. Takesaka, T. Nishioka, H. Kato, and M. Matsumura, J. Phys. Soc. Jpn. **79**, 083701 (2010).

[13] Y. Muro, J. Kajino, K. Umeo, K. Nishimoto, R. Tamura, and T. Takabatake, Phys. Rev. B **81**, 214401 (2010).

[14] J. Robert, J.-M. Mignot, G. Andre, T. Nishioka, R. Kobayashi, M. Matsumura, H. Tanida, D. Tanaka, and M. Sera, Phys. Rev. B **82**, 100404 (2010).

[15] D. D. Khalyavin, A. D. Hillier, D. T. Adroja, A. M. Strydom, P. Manuel, L. C. Chapon, P. Peratheepan, K. Knight, P. Deen, C. Ritter, Y. Muro, and T. Takabatake, Phys. Rev. B **82**, 100405 (2010).

[16] D. T. Adroja, A. D. Hillier. P. P. Deen, A. M. Strydom, Y. Muro, J. Kajino, W. A. Kockelmann, T. Takabatake, V. K. Anand, J. R. Stewart, and J. Taylor, Phys. Rev. B **82**, 104405 (2010).

[17] Y. Kawamura, S. Edamoto, T. Takesaka, T. Nishioka, H. Kato, M. Matsumura, Y. Tokunaga, S. Kambe, and H. Yasuoka, J. Phys. Soc. Jpn. **79**, 103701 (2010).

[18] A. Kondo, J. Wang, K. Kindo, T. Takesaka, Y. Ogane, Y. Kawamura, T. Nishioka, D. Tanaka, H. Tanida, and M. Sera, J. Phys. Soc. Jpn. **80**, 013701 (2011).

[19] H. Tanida, D. Tanaka, M. Sera, T. Nishoka, H. Kato, M. Matsumura, H. Harima, and H. Yasuoka, J. Phys. Soc. Jpn. **80**, 013708 (2011).

[20] J.-M. Mignot, J. Robert, G. Andre, T. Nishioka, R. Kobayashi, M. Matsumura, H. Tanida, D. Tanaka, and M. Sera, J. Phys. Soc. Jpn. **80**, SA022 (2011).

[21] K. Hanzawa, J. Phys. Soc. Jpn. **80**, 023707 (2011).

[22] S. I. Kimura, T. Iizuka, H. Miyazaki, A. Irizawa, Y. Muro, and T. Takabatake, Phys. Rev. Lett. **106**, 056404 (2011).

[23] S. Kimura, Y. Muro, and T. Takabatake, J. Phys. Soc. Jpn. **80**, 033702 (2011).

[24] A. Kondo, J. Wang, K. Kindo, Y. Ogane, Y. Kawamura, S. Tanimoto, T. Nishioka, D. Tanaka, H. Tanida, and M. Sera, Phys. Rev. B **83**, 180415(R) (2011).

[25] H. Kato, R. Kobayashi, T. Takesaka, T. Nishioka, M. Matsumura, K. Kaneko, and N. Metoki, J. Phys. Soc. Jpn. **80**, 073701 (2011).

[26] M. Matsumura, H. Tanida, D. Tanaka, H. Kato, T. Nishioka, and M. Sera, J. Phys. Soc. Jpn. **80**, 085001 (2011).

[27] H. Tanida *et al.* (unpublished).

[28] M. Takata, E. Nishibori, and M. Sakata, Z. Kristallogr. **216**, 71 (2006).

[29] M. Takaka, Acta Crystallogr., Sect. A: Found. Crystallogr. **64**, 232 (2008).

[30] Y. Kuroiwa, S. Aoyagi, A. Sawada, J. Harada, E. Nishibori, M. Takata, and M. Sakata, Phys. Rev. Lett. **87**, 217601 (2001).

[31] M. Sera, S. Itabashi, and S. Kunii, J. Phys. Soc. Jpn. **66**, 1548 (1997).

[32] M. Sera, N. Sato, and T. Kasuya, J. Phys. Soc. Jpn. **57**, 1412 (1998).

[33] K. Kaneko, N. Metoko, T. D. Matsuda, and M. Kohgi, J. Phys. Soc. Jpn. **75**, 034701 (2006).

[34] J. Yamaura and Z. Hiroi, J. Phys. Soc. Jpn. **80**, 054601 (2011).